Available online at www.sciencedirect.com
SCIENCE DIRECT®
Surface Science 544 (2003) 193–208
SURFACE SCIENCE
www.elsevier.com/locate/susc

High resolution photoemission study of growth, alloying, and intermixing of ultrathin ruthenium films on W(1 1 1) and W(2 1 1)

M.J. Gladys [a], G. Jackson [a], J.E. Rowe [b,c], T.E. Madey [a,*]

[a] *Department of Physics and Astronomy, Laboratory for Surface Modification, Rutgers, The State University of New Jersey, 136 Frelinghuysen road, Piscataway, NJ 08854-8019, USA*
[b] *Department of Physics, North Carolina State University, Raleigh, NC 27695, USA*
[c] *Army Research Office, Durham, NC 27703, USA*

Received 2 April 2003; accepted for publication 30 June 2003

Abstract

The alloying, intermixing, growth and faceting of ruthenium overlayers on tungsten single crystals have been studied with high resolution soft X-ray photoelectron spectroscopy, SXPS, (using synchrotron radiation) and low energy electron diffraction (LEED). W4f core-level photoemission spectra and W valence band spectra have been measured at various photon energies, and at normal and grazing emission angles, for W(1 1 1) and W(2 1 1). These two surfaces were chosen for this study because it has been shown previously that W(1 1 1) covered with monolayer films of several different 4d and 5d transition metals develop nanoscale pyramidal facets with (2 1 1) faces, upon annealing. The present work extends the measurement to another catalytically active overlayer metal, Ru. The growth and evolution for dosing and annealing on both W surfaces are investigated for coverages from 0 to greater than 3 monolayers of Ru (1 ML $= 1.7\times10^{15}$ atoms/cm^2). Incremental dosing of Ru causes intermixing of the Ru and W atoms at the interface, even at fractional monolayer coverages. Annealing of surfaces with Ru coverages > 1 ML produces a complex set of SXPS results that indicate the formation of surface Ru/W alloys. Faceting of Ru/W(1 1 1) is observed by LEED for Ru coverages > 1 ML, after annealing at temperatures between 700 and 1000 K. Upon annealing to temperatures higher than 1000 K, the SXPS data indicate that clustering of the Ru–W surface alloys may occur.

Keywords: X-ray photoelectron spectroscopy; Low energy electron diffraction (LEED); Growth; Ruthenium; Tungsten; Single crystal surfaces; Faceting; Alloys

1. Introduction

There is abundant recent evidence that adsorbed gases [1–3] and monolayer thin films of overlayer metals [4–8] can induce faceting of bcc W(1 1 1) and Mo(1 1 1) surfaces. Upon deposition of 1 ML of certain metals on W(1 1 1) and Mo(1 1 1) (including Rh, Ir, Pt, Pd, Au) and after annealing to $T > 800$ K, the initially planar surface converts to a faceted surface: three-sided pyramids having (mainly) bcc {2 1 1} faces with dimensions of ~10 nm or smaller cover the

* Corresponding author. Fax: +1-732-445-4991.
E-mail address: madey@physics.rutgers.edu (T.E. Madey).

0039-6028/$ - see front matter © 2003 Elsevier B.V. All rights reserved.
doi:10.1016/j.susc.2003.06.001

surface. The metal overlayer acts as a surfactant to alter the anisotropy of surface free energy; the pyramids are metal film-covered W (Mo), not crystalline aggregates of the overlayer.

Whereas many overlayer metals and other adsorbates cause faceting of W(1 1 1) and Mo(1 1 1), including Rh, Pd, Ir, Pt, Au, O, Cl [2–5,8,9] others do not (Ti, Cr, Fe, Ni, Ag, Cu, Gd) [4,10]. Che et al. have performed first principles calculations that address the materials specificity of faceting of W and Mo by ultrathin films [11]. They studied various metals grown on Mo(1 1 1) and W(1 1 1), and calculated the surface formation energies for film-covered (1 1 1) and (2 1 1) surfaces. They found that faceting of (1 1 1) to (2 1 1) is thermodynamically and kinetically allowed for 1 ML films of Au, Pd and Pt on Mo(1 1 1). Faceting is thermodynamically forbidden for 1 ML of Cu on Mo(1 1 1), and is thermodynamically allowed but kinetically blocked for Ag on Mo(1 1 1). The results of these calculations agree well with experiments to date.

An empirical correlation has been noted concerning the ability of overlayer elements to induce faceting [4]. All of the elements indicated in the previous paragraph to induce faceting of W(1 1 1) and/or Mo(1 1 1) have Pauling electronegativities > 2.0, whereas those that do not cause faceting have electronegativities < 2.0. This observation suggested that electronic structure plays a role in faceting. To search experimentally for possible electronic factors that influence faceting, we have used high resolution soft X-ray photoemission spectroscopy (SXPS) based on synchrotron radiation [12–15]. The aspect of SXPS that is most appropriate for this work is the fact that core-level electron binding energies of atoms at the surface or interface reflect the chemical environment of the atoms. Of particular use are measurements of the surface core-level shifts (SCLS) for the sharp 4f levels of W, Pt, etc. Whereas it is found that the SCLS is an extremely sensitive and useful indicator of interface formation, there is no clear correlation between Pauling electronegativity and surface or interfacial $4f_{7/12}$ binding energies [12]. This is not unexpected, since the Pauling electronegativity is a measure of initial-state charge transfer effects, while the measured 4f binding energies are influenced by a combination of initial- and final-state effects.

Another outcome of recent SXPS studies concerns the thermal stability of the overlayer films on W substrates [14,15]. For most systems studied (Rh, Pd, Ir, Pt, Au on W(1 1 1) and W(1 1 2)), we find evidence that a single monolayer of overlayer metal is thermally stable, and "floats" on the outer surface without significant alloy formation, for all temperatures up to the onset of desorption. For all systems except Au/W, we find that multilayer films form alloys upon annealing: invariably, W atoms from the substrate diffuse into the overlayer film, rather than vice versa. In certain cases (Pt/W, Ir/W) sharp 4f levels of both overlayer and substrate can be measured, to confirm evidence for alloy formation in multilayer films. In general, the alloying behavior of the bimetallic systems investigated is consistent with the known bulk phase diagrams (e.g., Pt is not soluble in W, but W is soluble in Pt to a maximum of ~60% W). Moreover, Born–Haber cycles and the equivalent core approximation (ECA) can be used to extract thermochemical data concerning energetics of adhesion, segregation and alloying in these systems [14].

The present paper focuses on the structure and thermal stability of Ru films on W(1 1 1) and W(1 1 2), as studied using LEED and SXPS. Ru is a metal of interest in catalytic applications, and an ultrathin Ru film > 1 ML on W(1 1 1) is found to induce faceting upon annealing to $T > 800$ K (note that the electronegativity of Ru is 2.2). However, atom exchange and intermixing at the Ru/W interface is seen for a fractional monolayer of Ru on either W(2 1 1) or W(1 1 1). This is in sharp contrast to other metal monolayers studied on W, which "float" on the outer surface upon annealing. The intermixing of Ru/W for low Ru coverages (<1 ML) and the formation of a Ru/W surface alloy for higher Ru coverages are consistent with the bulk phase diagram for which mixing of Ru in W is seen. A pairwise-interaction model of interfacial mixing has been developed to rationalize the measured SCLSs.

2. Experimental

The experiments were performed in an ultrahigh vacuum chamber, with base pressure better

than 1×10^{-10} Torr, on beamline U4A at the National Synchrotron Light Source. The photon energy used in this study was 80 eV for the W(1 1 1) and 130 eV for the W(2 1 1), with nominal resolution of 50 and 100 meV, respectively. A VSW 100 mm mean radius hemispherical energy analyzer of 5° angular resolution collected the photoelectrons with pass energy of 2 and 5 eV for W(1 1 1) and W(2 1 1), respectively. This gives a nominal resolution of 44 and 90 meV, and a total instrumental resolution of approximately 65 and 135 meV for the W(1 1 1) and W(2 1 1), respectively. The photon flux is measured continuously and the XPS spectra shown here are normalized to account for gradually varying photon flux.

The samples were cleaned by repeated cycles of annealing in 1×10^{-7} Torr oxygen at 1200 K for 5 min, followed by flashing to ~2300 K. The cleanliness was verified by XPS and LEED. The temperature was measured using W5%Re–W26%Re thermocouple wires that were spot-welded to the tungsten crystals.

The ruthenium overlayers were prepared by thermal evaporation of Ru onto the sample held at room temperature (300 K). The Ru source consisted of high purity Ru powder in an e-beam heated Ta crucible; after thorough outgassing, the Ru powder sintered and the evaporation rate during heating was reproducible. The incremental deposition of the ruthenium onto the tungsten surfaces was monitored by measuring changes in work function and the attenuation of the W4f photoemission peak. The details of these procedures are discussed in detail elsewhere [13,14]. Work function changes were measured by biasing the sample to −9 V and scanning the photoemission threshold. The photoemission spectra of $W4f_{7/2}$ were taken immediately after each dose of Ru. To investigate the transformation in the overlayer and interface during heating, stepwise annealing to increasingly higher temperatures is used. The sample was allowed to cool after each anneal step and SXPS spectra and LEED were recorded. A monolayer (ML) is defined as a 'physical monolayer', the coverage for which every exposed W substrate atom is covered by a Ru atom (1.73×10^{15} atom cm^{-2} for W(1 1 1); 1.63×10^{15} atom cm^{-2} for W(2 1 1)). The coverage determination was confirmed by the observation that faceting is induced only if at least a physical monolayer of the overlayer film covers the surface locally. This phenomenon has been seen with all the previously studied overlayer metals that have shown to induce faceting [4,13,16], and is consistent with the ruthenium overlayer investigation presented here.

At a photon energy of 80 eV, the $W4f_{7/2}$ photoemission is very surface sensitive and therefore surface features have substantial visibility. The annealing and dosing core-level spectra were taken at normal emission. The use of different photon energies and different emission angles assist in the analysis of the measured core-levels, via their effects on the attenuation of features within the $W4f_{7/2}$ core level spectra. For example, higher photon energies (>130 eV) provide more bulk information since the $W4f_{7/2}$ electrons have higher kinetic energy, and therefore can escape from greater depth below the surface. Grazing emission (70° from surface normal) provides more surface information, since at grazing angles the electrons from the bulk are attenuated more effectively than electrons emitted perpendicular to the surface. In this study, the analysis of the $W4f_{7/2}$ core-level photoemission spectra involved a non-linear least squares fitting procedure. It was assumed that each $W4f_{7/2}$ core-level feature has a Doniach–Sunjic lineshape [12,13,17]. The parameters used with this lineshape are the Lorentzian linewidth, Gaussian linewidth, and the asymmetry parameter from the creation of core holes during photoemmision.

3. Results

3.1. W(1 1 1)

A $W4f_{7/2}$ core-level photoemission spectrum for clean W(1 1 1) is shown in Fig. 1. The dominant surface features clearly demonstrate the surface sensitivity that can be obtained at 80 eV photon energy and also indicates the cleanliness of the tungsten surface. The clean spectrum agrees with that observed by Tao et al. [12] and with earlier measurements [18]. The three distinct $W4f_{7/2}$ features shown in Fig. 1 are assigned [12] as the bulk,

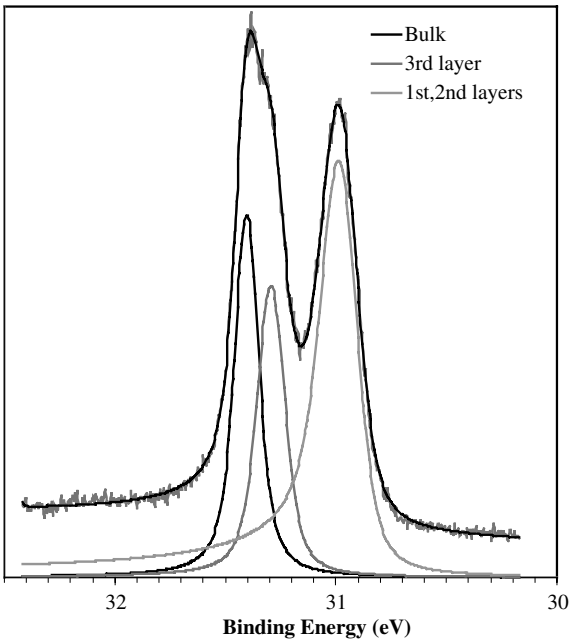

Fig. 1. Clean W(1 1 1) core-level photoemission spectra taking with 80 eV photon energy. Fitting parameters are: Natural linewidth of 76 meV, Gaussian width of 100 meV, asymmetry parameter of 0.02. Surface binding energy shifts with respect to bulk are −440 meV for the combined first and second layer peak and −140 meV for the third layer.

the third surface layer (which has a −140 meV core-level shift with respect to the bulk), and the unresolved first and second layers with a core-level shift of −440 meV with respect to the bulk $W4f_{7/2}$ core-level. It is noteworthy that the combined intensities of the surface $W4f_{7/2}$ core-level features are greater than that of the bulk $W4f_{7/2}$, due to the shallow mean free path of emitted photoexcited electrons.

To assist in the assignment of the bulk and surface features in the fitting procedure, spectra were measured at different photon energies (higher photon energies produce lower surface sensitivity and therefore the bulk peak becomes more pronounced). In addition, changing the angle of emission from normal to grazing increases the relative intensity of the surface features. Fig. 2 compares the $W4f_{7/2}$ photoemission spectra for normal and grazing emission. The relative increase in intensity of the surface features with respect to the bulk peak at grazing emission confirms identification of the surface peaks.

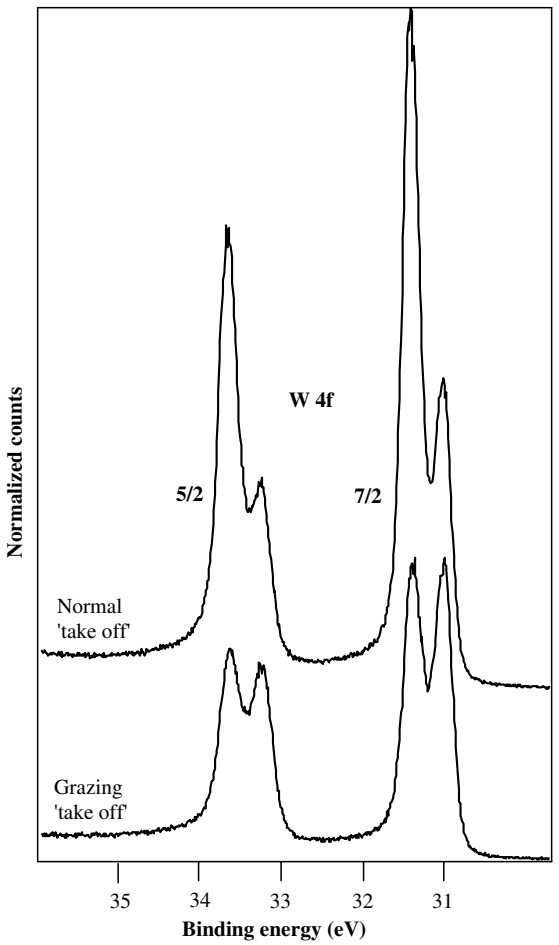

Fig. 2. Comparison of W(1 1 1) photoemission curves for normal and grazing emission. The grazing spectrum has much lower intensity due to a lower cross-section at this angle. Note the increase in the surface to bulk peak ratio as a result of the increase in surface sensitivity.

3.1.1. Dose dependence

The surface features in the $W4f_{7/2}$ photoemission are due to atoms at the metal/vacuum interface. These atoms experience a different electronic environment from the bulk W atoms that are completely surrounded by other W atoms. If the clean W(1 1 1) surface is covered with a ruthenium overlayer, the W–vacuum interface is replaced with a W–Ru interface and changes in the photoemission spectrum are expected: A W atom at the Ru/W(1 1 1) interface experiences a different chemical environment from a W atom at the vac-

uum/W(1 1 1) interface. Fig. 3 shows series of $W4f_{7/2}$ spectra accompanying a dosing sequence for up to 2 ML of Ru on W(1 1 1). A dose time of 30 min corresponds to a coverage of one physical monolayer (1 ML). The surface features are suppressed by even small amounts of Ru and are also shifted to higher binding energies. On the high binding energy side of the bulk feature a small feature is also detected.

An example of a fitted Ru-dosed $W4f_{7/2}$ core-level spectrum is shown in Fig. 4, for a 1 ML dose. The parameters used in the fitting are linewidth 76 meV, Gaussian width of the bulk feature of 100 meV, and an asymmetry value of 0.02. The Gaussian widths for the high binding energy peaks are 300 meV. The peak on the higher binding energy side of the bulk peak labeled "interface" is identified with the W–Ru interface [12]; it is located at approximately 66 meV from the bulk. The small feature on the lower binding energy side corresponds to surface W atoms that have small interaction with the deposited Ru, and has a binding energy of −230 meV relative to the bulk. The peak located at a binding energy shift of +380 meV from the bulk is identified as the intermixing peak arising from an exchange of the Ru and W atoms at the interface.

In the discussion following, we refer to Ru-induced features with higher binding energy as

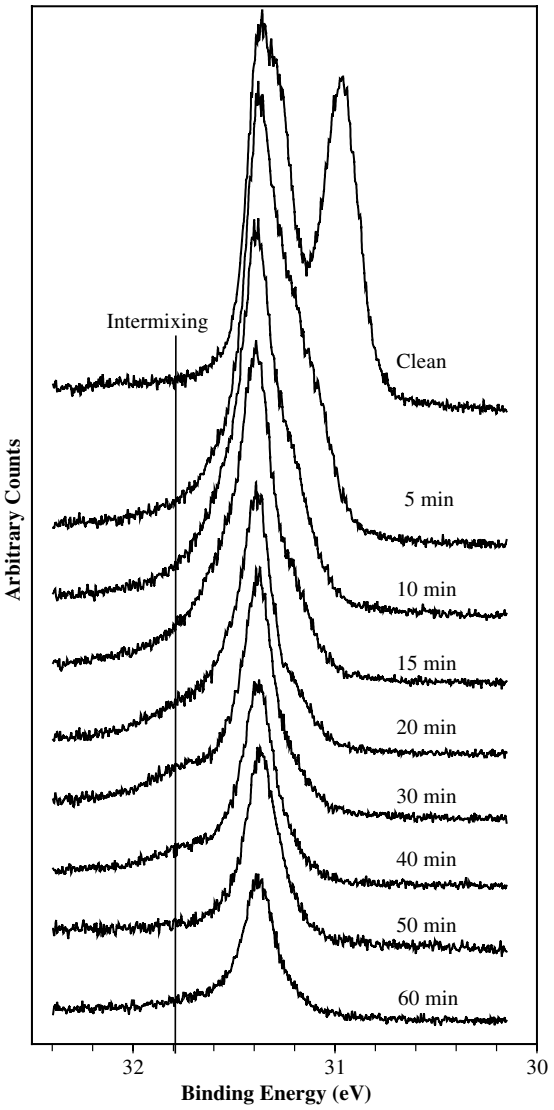

Fig. 3. Dosing sequence of $W4f_{7/2}$ core-level spectra for up to 2 ML of Ru on W(1 1 1). Surface features are suppressed and shift towards the bulk peak. Intermixing of sub-monolayer is indicated by the extra feature on the high binding energy side of the bulk tungsten peak. A 30 min dose corresponds to a coverage of 1 physical monolayer (1 ML).

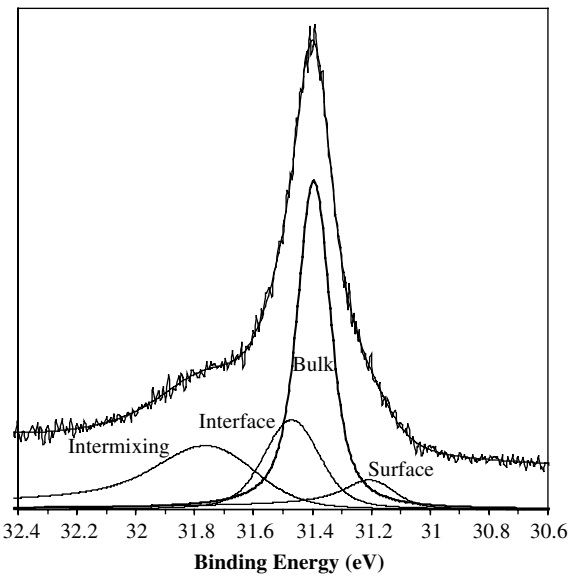

Fig. 4. Non-linear least squares fit of the SXPS spectrum of the 1 ML dose of Ru on W(1 1 1). The Gaussian widths for the bulk peak are the same as stated in Fig. 1. The Gaussian widths of the high binding energy peaks are 300 meV, suggesting the possibility of more unresolved features within the high binding energy peaks from interactions in different W layers.

"intermixing" or "alloy" peaks. The distinction between intermixing and alloy formation is not a rigid one. We define intermixing as an interchange of atoms at the Ru–W interface; this is probably a metastable configuration that is characterized by new W4f features that appear at higher binding energies when Ru is dosed at ~300 K, and can be associated with coverages $\leqslant$ 1 ML. Alloy formation is associated with annealing of Ru coverages > 1 ML, and may closely resemble bulk alloy formation. At coverages ~ 1 ML, both intermixing and alloy formation can be seen. In previous studies in our laboratory, Kolodziej et al. [14,15] observed alloy features for multilayers of overlayer metals (Pd, Rh, Ir, Pt) on W(1 1 1) and W(1 1 2); intermixing for coverages $\leqslant$ 1 ML was seen only for Ir/W(1 1 1).

Fig. 5 is a plot of intensity of the fitted spectra of Fig. 3, using the same fitting parameters (Gaussian and Lorentzian linewidths, and asymmetry parameter) as in Fig. 4. Binding energy changes of the peaks as a function of dose were constant to within 2% (except the intermixing peak, see below). The intermixing peak has a maximum at 1 ML coverage, which we associate with W atoms diffusing into the Ru layer; this feature is suppressed upon further Ru dosing. Another interesting characteristic of Fig. 5 is the exponential relationship of the bulk peak with coverage indicating a form of layer growth. The binding energy of the intermixing peak exhibits non-monotonic behavior as Ru coverage increases. Initially the intermixing peak increases in binding energy as a function of coverage, and then remains constant up to 1 ML. At this point there is a dramatic decrease in binding energy (~100 meV), possibly caused by the second layer covering the intermixed layer at the W–Ru interface.

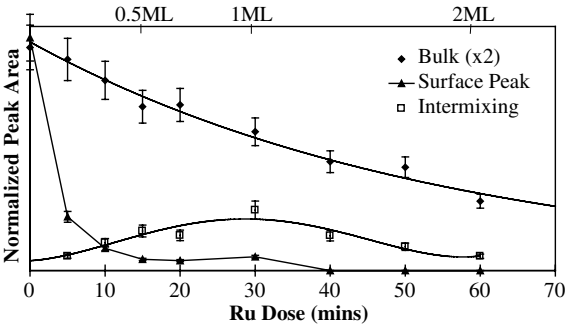

Fig. 5. Least-squares fitting analysis of the integrated intensity change during dosing of Ru on W(1 1 1). The bulk peak attenuation indicates a form of layer growth while the intermixing peak maximizes at approximately 30 min dose (1 ML coverage), above which it decreases in both intensity and binding energy.

3.1.2. Annealing effects

W4f spectra associated with an annealing sequence for less than 1 ML of Ru/W(1 1 1) are presented in Fig. 6. LEED studies displayed no faceting of this surface, however at 800 K peaks at higher binding energy than the bulk are observed. These peaks (labeled "intermixing") have binding energy shifts of 400 and 550 meV larger than the bulk peak. The observation of higher binding energy W4f features due to atomic intermixing for

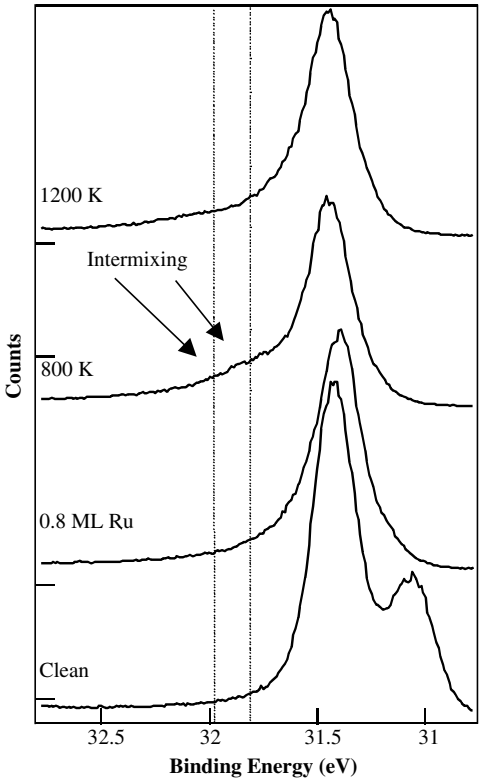

Fig. 6. Annealing sequence for fractional monolayer Ru on W(1 1 1). High binding energy peaks are observed, and are due to intermixing of the surface atoms. No faceting of the substrate is observed with coverages below 1 ML.

Ru coverages < 1 ML in Figs. 3 and 6 is a novel aspect of this work: for other overlayers (Rh, Pd, Pt,...) intermixing is seen only for coverages greater than 1 ML, i.e., for coverages greater than the minimum needed to induce faceting [13–15].

For coverages higher than 1 ML, complete faceting of the surface is observed with LEED at approximately 850 K. A comparison of LEED patterns for the planar and faceted W(1 1 1) is shown in Fig. 7. Fig. 7a is the sharp (1 × 1) pattern characteristic of the clean W(1 1 1) surface. The three signature facet spots are clearly visible around the (1 × 1) spots, as shown in Fig. 7b. This faceting pattern is generated by dosing the sample with 2 ML of Ru and then annealing to 900 K. The identification of LEED patterns from faceted surfaces is described in more detail by Song et al. [19,20]. LEED beams from a faceted substrate do not move radially with the (1 1 1) spots when the energy is changed. Instead, the faceted spots move through the (1 1 1) spots making smaller or larger triangles depending on the change in energy; they converge on points identified as specular beams due to electron scattering of the incident electrons from Ru-covered W(1 1 2) facets. The faceting LEED spots progressively sharpen with increasing temperature up to approximately 1000 K, and the (1 × 1) spots become increasing diffuse. Higher temperatures caused the faceting spots to become more diffuse also until they disappear at 1300 K. The (1 × 1) spots gradually sharpen as the temperature is increased further until the original clean LEED pattern is reached when the sample is flashed clean at 2300 K. Faceting is seen for Ru coverages > 1 ML, although Fig. 7b corresponds to 2 ML.

A more detailed look at the Ru-induced changes in the $W4f_{7/2}$ core level is shown in Fig. 8 for an initial coverage of 2 ML. These data reveal a complex sequence of events taking place in the annealing sequence before, during and after faceting. By analogy with data for alloy formation in other metal layers on W [14,15], a peak we identify with a surface alloy, P1, forms with a binding energy shift of 790 meV from the bulk peak in the first anneal at 600 K. Peak, P2, appears at 700 K and has an initial core-level shift of 450 meV from the bulk peak. Faceting is observed between 750 and 1300 K. The LEED pattern shows an optimally faceted surface (i.e. faceting spots are sharpest and brightest) at 1000 K. Temperatures higher than 1300 K cause desorption of the ruthenium. This completely destabilizes the facets and the surface reverts back to the planar (1 1 1).

An analysis of the annealing sequence of Fig. 8 for the 2 ML dose on W(1 1 1), based on the Doniach–Sunjic fitting procedure, is shown in Fig. 9; here we plot the integrated intensities of the

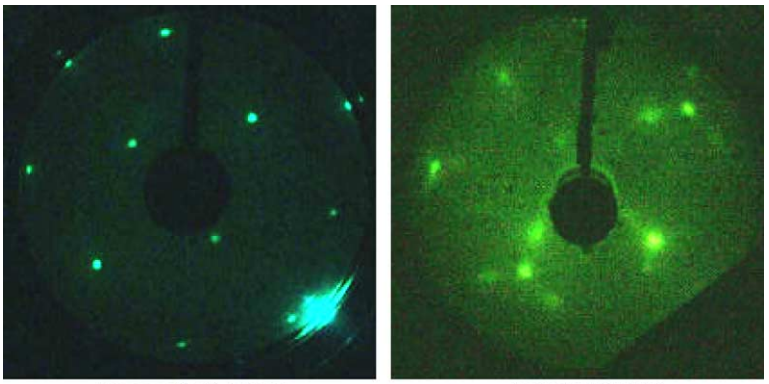

Fig. 7. Comparison of LEED patterns for (a) planar and (b) faceted W(1 1 1). The three spots in a triangle in (b) are the signature pattern for a pyramidal faceted surface. The three spots move radially in or out from the center of the triangle with changes in electron energy. From this pattern, the sides of the pyramids have been previously determined to be {2 1 1} faces.

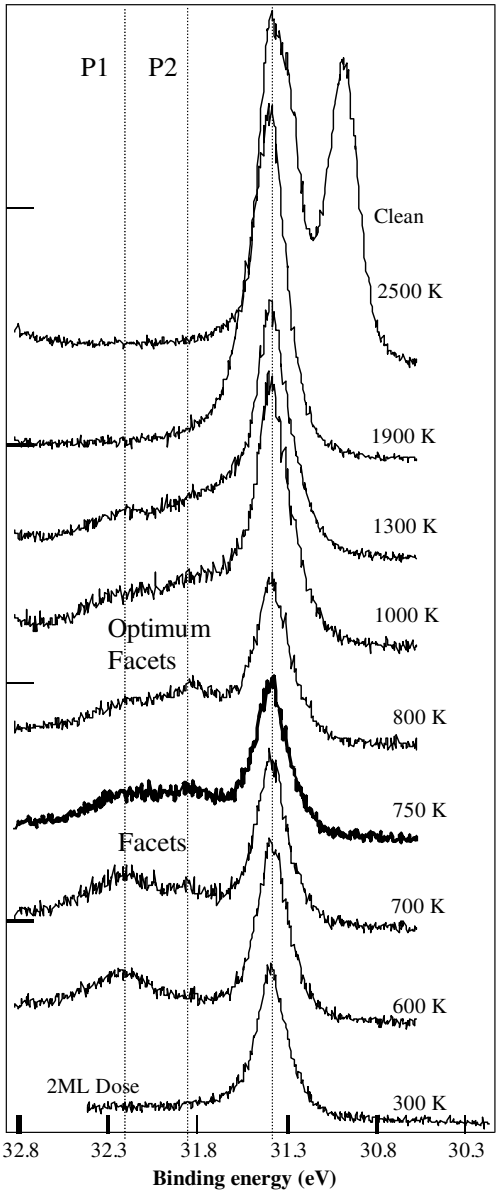

Fig. 8. $W4f_{7/2}$ core-level photoemission spectra accompanying annealing of 2 ML Ru on W(1 1 1). Stable alloy features are observed at higher binding energies than the bulk, before, during, and after faceting of the substrate. Faceting of the substrate occurs at $T \geqslant 750$ K.

fitted components vs. annealing temperature. Peaks P1 and P2 are the features that start forming at temperatures around 600 K. These two peaks maximize in the temperature range at which the

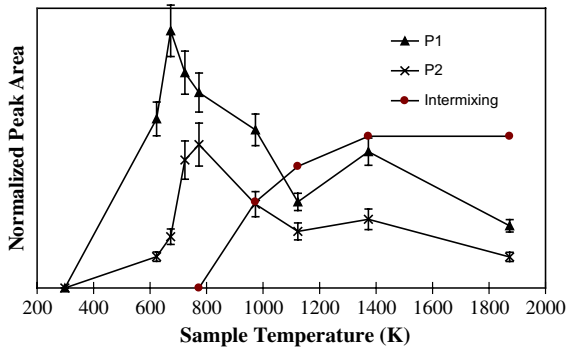

Fig. 9. Least-squares-fitting analysis of the 2 ML Ru/W(1 1 1) annealing sequence. The graph reveals a complex set of events occurring over a wide range of temperatures. The alloy peaks reach maximum intensity in the temperature range where faceting is observed. A third peak begins to grow at 1000 K with a binding energy shift of 290 meV.

faceting mechanism is initiated. In addition, at a temperature of ~1000 K, another peak arises with a similar binding energy (290 meV) as the intermixing peak in the dosing sequence (Fig. 3). Although the intermixing peak is not apparent in the raw data for the annealing sequence (Fig. 8), it is necessary to include this feature in order to fit the data. This phenomenon is discussed later.

To examine the influence of oxygen on a Ru covered W surface, 50 L of O_2 was adsorbed onto both clean W(1 1 1) and multilayer Ru-covered W(1 1 1) surfaces. Fig. 10 shows a comparison of core-level shifts observed for these conditions. Large binding energy shifts are observed for O_2 adsorbed onto the Ru covered surface (the $4f_{7/2}$ features are shifted by ~2 eV), whereas O_2 on clean W(1 1 1) reveals small shoulders on the high binding energy side of the respective $4f_{5/2}$ and $4f_{7/2}$ bulk features. This enhancement is suspected to be due either to Ru catalytically activating the O_2 on W to form oxides or to a ternary RuWO alloy formed even at room temperature. The top curve, corresponding to a slightly annealed oxygen + Ru covered W(1 1 1) substrate, shows changes at temperatures as low as 300 °C.

3.2. W(2 1 1)

The clean $W4f_{7/2}$ spectrum for W(2 1 1) is shown in Fig. 11. In contrast to the W(1 1 1)

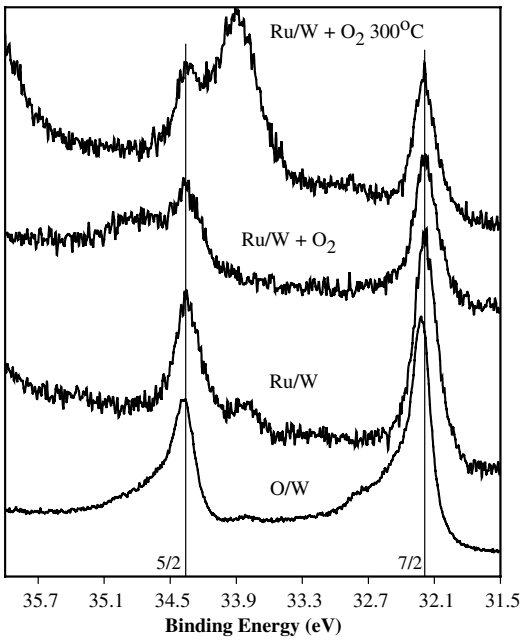

Fig. 10. Effect of oxygen on Ru covered W(1 1 1) surfaces. W4f spectra are stacked vertically to compare $Ru/W + O_2$, $Ru/W + O_2$ 300 °C, Ru/W and O/W where W refers to W(1 1 1) surface. Significant positive binding energy shifts are observed with oxygen covered Ru/W surfaces. This shift is considerably amplified when the surface is heated to temperatures as low as 300 °C.

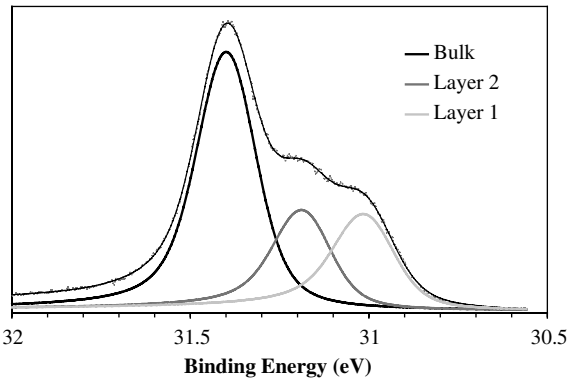

Fig. 11. Clean $W4f_{7/2}$ core-level photoemission spectrum for W(2 1 1). Two surface features are resolved for the two outer surface layers and are located at −220 and −375 meV from the bulk. Note the significantly different structural change from the W(1 1 1) surface, Fig. 1.

surface (see Fig. 1), the core-level shifts of the first and second layers on the W(2 1 1) surface are smaller. The binding energy shifts of the first and second layer are −220 meV and −375 meV, respectively, from the bulk. The Gaussian widths of the surface and bulk peaks are larger than the widths measured for W(1 1 1), as described by Tao et al. [12]. Additionally, the W(2 1 1) bulk peak has a larger Gaussian width than the surface features, as was also seen by Kolodziej et al. [14]. This behavior is different from the W(1 1 1) 4f photoemission and cannot be explained by electron–phonon scattering alone. It has been suggested that this inhomogeneous broadening is due to relaxation in the surface region [12]. The analysis of data for Ru on W(2 1 1) is similar to that for W(1 1 1).

3.2.1. Dose dependence

A series of $W4f_{7/2}$ spectra accompanying a dosing sequence for Ru on W(2 1 1) is shown in Fig. 12. An intermixing feature appears at approximately 0.5 ML of Ru, with a core-level shift of +360 meV relative to the bulk feature. This is similar to the behavior of Ru/W(1 1 1), as shown in Fig. 3. The Ru-dose dependence of the intermixing peak is shown in Fig. 13; the data of Fig. 12 were fit using a non-linear least squares procedure. The estimated exponential decay of the bulk peak is consistent with layerwise growth on the surface and the initial stages of the bulk peak intensity of Fig. 13 are not significantly different from the W(1 1 1) data in Fig. 5.

3.2.2. Annealing effects

The $W4f_{7/2}$ spectra for an annealing sequence of a multilayer covered W(2 1 1) surface are presented in Fig. 14. Complex alloying features also appear in the W4f spectra for this surface, consistent with the W(1 1 1) (cf. Fig. 9); an exception is the large peak, labeled P, with a core-level shift of 880 ± 20 meV. This peak has a large intensity at 700 K and is evident at temperatures as low as 550 K. Between 700 and 800 K a structural change takes place on the surface: the evidence is that peak P changes binding energy or disappears completely while another develops with a binding energy shift of +750 meV. Alloy peak P2, with a binding energy shift of 290 meV, develops when the temperature reaches the region that faceting of the

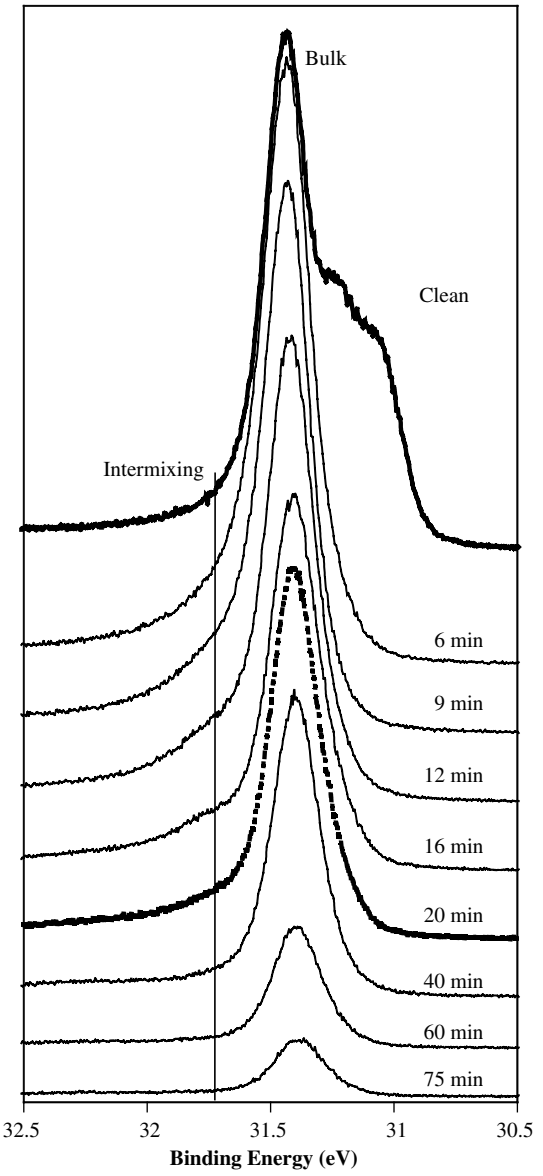

Fig. 12. W4f$_{7/2}$ core-level spectra for a dosing sequence of Ru on W(2 1 1). An intermixing peak is also observed, whose intensity maximizes at 1 ML coverage similar to the W(1 1 1) case.

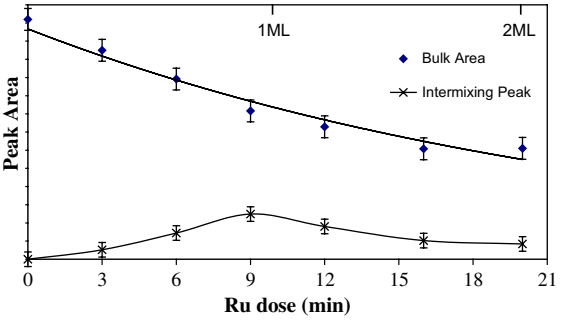

Fig. 13. Analysis of the intensity changes for the observed features in the dosing sequence of Fig. 12 for Ru on W(2 1 1). The attenuation of the bulk peak is consistent with layer growth while the intermixing feature is observed to maximize at approximately 1 ML.

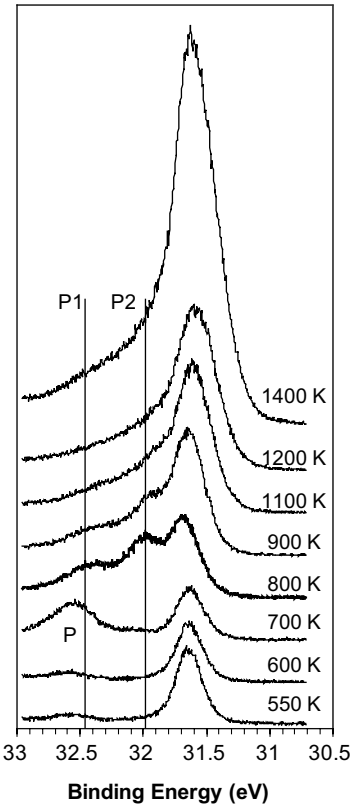

Fig. 14. W4f$_{7/2}$ core-level photoemission spectra accompanying an annealing sequence for Ru/W(2 1 1). As for W(1 1 1) (cf. Fig. 8) the alloy features are a prominent feature throughout the temperature region where faceting of the substrate occurs. Three alloy features are present and change considerably with increasing temperature, suggesting a rearrangement of the surface atoms.

W(1 1 1) is observed with LEED. Fig. 15 shows the non-linear least squares fit for the 800 K W4f$_{7/2}$ spectrum in the annealing sequence in Fig. 14. The peak P1, observed above 700 K, has a similar binding energy to the peak P1 found in the annealing sequence of multilayer Ru on W(1 1 1) (see

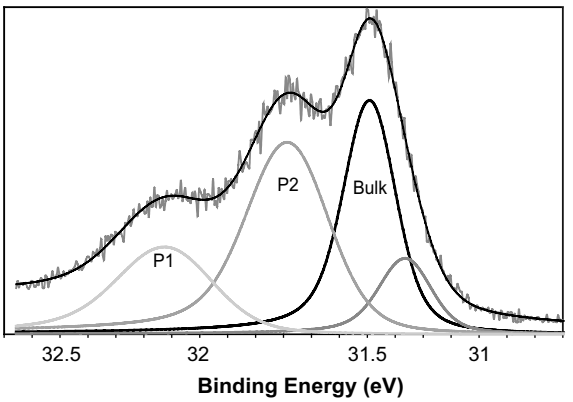

Fig. 15. A fitted SXPS spectrum for multilayer dose of Ru on W(2 1 1) annealed to 800 K. Two large alloy features dominate the $W4f_{7/2}$ spectrum with binding energy shifts of 770 meV (P1) and 290 meV (P2) from the bulk.

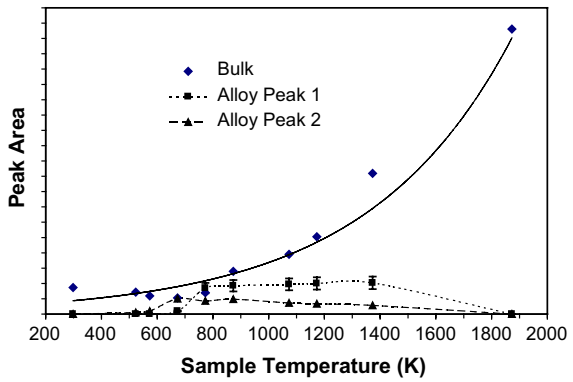

Fig. 16. Analysis of intensity changes for Ru/W(2 1 1), annealing sequence of Fig. 14; peak area versus annealing temperature. Alloy features remain relatively constant until the onset of desorption of ruthenium at approximately 1400 K. Bulk peak growth occurs well before Ru desorption, indicating cluster formation on the surface.

Fig. 9). However the alloy peak, P2, has a difference of binding energy shift of the amount of −160 meV from the similar alloy peak (P2 in Fig. 9) observed for the W(1 1 1) system. The integrated peak intensity versus annealing temperature is shown in Fig. 16 for the annealing sequence in Fig. 14. The bulk peak intensity increases monotonically upon heating to temperatures > 570 K, whereas the alloy peaks appear at 300 °C and remain relatively constant until 1400 K. The growth of the bulk peak at temperatures well below the onset of desorption may indicate that overlayer Ru clusters form on the surface, perhaps as a Ru/W alloy.

4. Discussion

The ruthenium-covered W surfaces demonstrate unusual characteristics compared to previously studied overlayers of Pd, Pt, Ir, Ru on W(1 1 1) and W(2 1 1). First principles calculations of surface segregation energies by Ruban et al. [21] predict a strong tendency for segregation of Pt, Pd and Ru on tungsten. Surface segregation of Pd and Pt overlayers is consistent with the corresponding bulk phase diagrams illustrating minimal solubility for temperatures below 1000 °C. This was confirmed in SXPS studies of Pt, Pd, and Rh monolayers on W(1 1 1) and W(2 1 1), [14,15] where no evidence for intermixing or alloying of single monolayer films with W was observed. In only one case of a single monolayer film, Ir on W(1 1 1), is there evidence of possible intermixing upon annealing, but the effect on W4f SCLSs is more subtle than seen here for Ru/W. Intermixing and alloying is seen, however, for multilayers of Pt, Rh, and Ir on atomically rough W(1 1 1) even at 300 K, while only Pt was observed to intermix and alloy on W(2 1 1) at 300 K. The dilute intermixing observed while dosing approximately 1 ML of Ru on both the W(1 1 1) and W(2 1 1) surfaces (cf. Figs. 3 and 13) indicates a low segregation energy for the Ru–W interface.

An atomic arrangement in which a tungsten atom has non-tungsten nearest neighbor atoms results in core-level shifts between the bulk W peak and the peak due to a single W atom partially or completely surrounded by Ru. Tungsten atoms entirely surrounded by non-tungsten atoms are anticipated to undergo a maximum core-level shift. However, the mechanisms that dominate core-level shifts in transition metals are somewhat complicated. Some of the factors include charge transfer, rehybridization of valence orbitals, changes in final-state screening, Madelung potential terms, and reference level shifts [22]. Transition metals have two types of electrons that participate

in bonding: d- and sp-like. Transition metal alloying results in an interaction between s, p and d band effects. Late transition elements often lose d-like electrons when alloyed with early transition metal elements [23]. The hybridized d orbitals directly interact with the 4f orbitals and increase the binding energy of electrons from the 4f core-level.

A previous discussion by Kolodziej et al. [14] described the interaction between Pt or Ir overlayers and W substrates. Based on the electronegativity differences of Pt, Ir and W, charge transfer from W to Pt (Ir) is likely. Alloying of Pt and W causes both Pt4f and W4f peaks to shift to higher binding energy than the bulk feature. With Ir on W, however, the W4f binding energy changes but the Ir 4f energy does not change significantly. This reveals that interatomic charge transfer does not dominate the core-level shifts in transition metal alloying.

Since the p and d core-level photoemission from Ru have such large intrinsic widths, it is difficult to measure exact core-level shifts. We observed the Ru peak during dosing and annealing, and found no measurable core-level shift to within 100 meV. Since little or no core level shift occurs for Ru/W, as in the case of Ir/W, it is possible that charge transfer occurs for the s and p orbitals but the d orbital occupancy is not changed. Apparently the effects that contribute to possible Ru core-level shifts cancel to produce a net zero outcome when Ru interacts with W. The complex behavior observed for the W4f features implies many or all of the factors causing core-level shifts are playing some role.

The W atoms that diffuse into the Ru overlayer upon deposition at 300 K encounter a barrier as more Ru is deposited. As the Ru coverage increases above 1 ML, the intermixing signal is attenuated, indicating that W atoms do not diffuse further into the overlayer during deposition at 300 K. First principles calculations using the LMTO-CPA method by Christensen et al. [24] suggest a small surface mixing energy for the Ru–W system (Ru impurity on W substrate). The low temperature intermixing observed for Ru/W is consistent with the bulk phase diagram of Ru and W shown in Fig. 17. First, the solubility of W atoms in Ru is very high even at low temperatures, so it is energetically favorable for W atoms to diffuse into the Ru overlayer and form stable phases or alloys. There is one sizable difference between the Ru–W bulk phase diagram and the Pt–W, Pd–W, etc., bulk phase diagrams. That is, the extended region of Ru/W solubility on the right of the phase diagram in Fig. 17 at high W concentrations indicates some solubility of Ru in W at high temperatures. This is very different from Pd/W, Pt/W, etc., for which the solubility of Pd, Pt, etc. is much more limited. However, little Ru is able to diffuse into the W bulk from the deposited overlayer at 300 K even though diffusion of Ru into W may occur at higher temperatures. Additionally, the Ru–W bulk phase diagram includes a region of stoichiometric alloy in addition to solid solution.

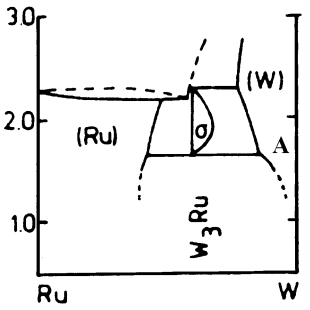

Fig. 17. W–Ru bulk phase diagram [5]. Notice the high solubility of W in Ru even at low temperatures.

Additional alloy features appear in the $W4f_{7/2}$ spectra when the Ru dosed W surface is annealed. Two alloy peaks arise during the annealing sequence for both W(1 1 1) and W(2 1 1) (cf. Figs. 8 and 14) at temperatures as low as 550 K. This temperature is high enough for W atoms to overcome the diffusion barrier and form an alloy with the rest of the Ru film. The temperature at which ruthenium atoms desorb from tungsten has not been precisely determined, but we estimate it to be between 1500 and 1600 K. The XPS analysis of the bulk feature during the annealing sequence for the W(1 1 1) surface (Fig. 7) reveals a substantial increase in bulk signal in the temperature range 1330–1450 K. The fluctuations and increase of W4f intensity measured as a function of temperature below the desorption threshold suggest a complex restructuring on the surface. The intensity increase of the bulk feature may be a result of

clustering of Ru–W alloys since more substrate W atoms are uncovered and a higher photoemission yield from substrate atoms is observed. Cluster formation has been seen by Kolodziej et al. [14,15] for Pt and Pd overlayers on W(1 1 1) but not on W(2 1 1). Coverages of Ru less than 1 ML on both W(1 1 1) and W(2 1 1) also produce identical alloy peaks at similar temperatures. This may indicate formation of Ru/W alloy islands. Previous observations by Nien and Madey [25] show that 1 ML of overlayer Pd coverage is sufficient to cause faceting and that extra Pd atoms form three-dimensional clusters upon annealing.

The W(1 1 1) multilayer annealing sequence (Fig. 9) also reveals a reappearance of the intermixing peak with a SCLS of 300 meV from the bulk peak, between 700 and 1600 °C. Since the intermixing peak (which maximizes at 1 ML in the dosing sequence) is a consequence of the vacuum–Ru–W environment; the reoccurrence of this peak seems to be a result of uncovering of the interface accompanied by 3-D clustering of W–Ru alloys. The reappearance of the intermixing peak has also been observed by Kolodziej et al. [15] for 1 ML of Ir on a W(1 1 1) surface. When annealing to low temperatures, an intermixing peak is observed and is associated with an intermixed, reconstructed, planar W(1 1 1) surface. However, this Ir/W feature disappears when the sample is annealed to temperatures that induce faceting, but higher temperatures that induce both faceting and planar surfaces to coexist cause the Ir/W intermixing peak to reappear. This is very similar to the reappearance of the intermixing feature when Ru is on the surface and reinforces the previous suggestion that planar regions coexist with clusters of W–Ru alloys.

5. Model of surface core-level shifts

To provide more understanding into the tungsten SCLS observed with Ru overlayers, a simple model has been developed to help interpret the W4f features. This model does not give quantitative predictions of binding energy shifts observed for the Ru–W system, but merely provides a qualitative explanation of possible changes in atom positions that might produce core-level shifts. Fig. 18 shows a clean W(1 1 1) surface, illustrating the three surface layers as indicated. In this model, we consider the effect of the surrounding atoms and the vacuum interface. Bcc W bulk atoms have coordination 8, which means that there are 8 W nearest-neighbor atoms. The bulk atoms also have 6 next nearest-neighbor atoms, which may contribute to SCLSs. To keep this coordination comparative to bulk atoms when considering surface W atoms, equivalent imaginary "vacuum atoms" are created to approximate the missing nearest-neighbor and next nearest-neighbor atoms caused by the vacuum interface. The "vacuum atoms" are only representative of the vacuum interface, where the effect of the vacuum would not be localized at a coordination site but rather distributed across the surface atoms. Therefore nearest-neighbor and next-nearest-neighbor imaginary "vacuum atoms" may have the same effect on the surface atoms.

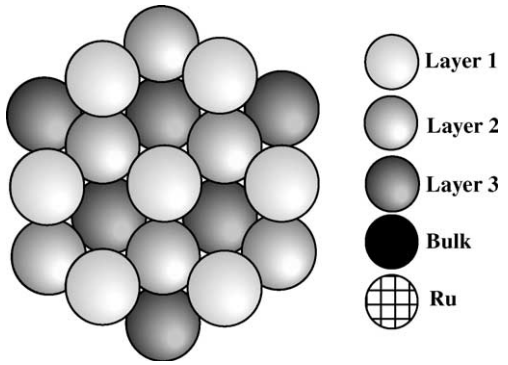

Fig. 18. Schematic diagram of the W(1 1 1) surface, top view. The diagram illustrates the three outer surface layers.

The coordination for clean unreconstructed W(1 1 1) is given below:

$$\text{Layer 1} = 4W_{NN} + 3W_{NNN} + 4Vac_{NN} + 3Vac_{NNN}$$
$$\text{Layer 2} = 7W_{NN} + 3W_{NNN} + 1Vac_{NN} + 3Vac_{NNN}$$
$$\text{Layer 3} = 7W_{NN} + 6W_{NNN} + 1Vac_{NN}$$

where NN indicates nearest-neighbor atoms and NNN are next-nearest-neighbor atoms. Vac represents the imaginary "vacuum atoms". In the clean W4f spectrum of W(1 1 1) in Fig. 3, the surface features identified with layers 1 and 2 are

shifted to lower binding energy by a large amount. This is represented by the interaction with the Vac atoms in the clean W(1 1 1) model. The first layer is shifted the most since it interacts with 7 Vac atoms whereas the second and third layers interact with 4 and 1 "Vac atoms" respectively. Layers 2 and 3 also interact with more tungsten atoms, which has the tendency to shift their core-levels to higher binding energies.

Models for 1/3, 2/3 and 1 ML monolayer coverages have been constructed and it is found that even at monolayer coverage the largest number of Ru atoms that interact with surface W atoms is 4 nearest neighbors and 3 next nearest neighbors. Furthermore, interactions with nearest-neighbor W atoms reduce the probability that the W SCLS is large enough to correspond to the observed W4f feature in Fig. 4. A Ru interaction of this type could, however result in an interface peak observed close to the bulk peak (Fig. 4), at a binding energy shift of 230 meV. Due to the high mutual solubility of the Ru–W system, intermixing at the interface occurs upon annealing. To model the interactions of possible intermixed species, a simple interchange method was adopted for 1 and 2/3 ML coverage. Figs. 19 and 20 are illustrations of the interchange model for 1 and 2/3 ML coverage. The 1 ML result is particularly interesting when the second layer W is interchanged with the Ru atom on top. In this case, the first and second layer W atoms interact with seven Ru nearest- neighbor atoms. This large Ru interaction may be expected to cause the $W4f_{7/2}$ core-level to shift to a binding energy greater than that of the bulk W. We suggest that this may be the origin of the feature on the high binding energy side of the bulk peak in the dosing sequence in Fig. 3. Additionally, the schematic of this configuration in Fig. 19c shows what seems to be a stable Ru–W phase with alternate rows of three Ru and three W atoms. Based on the model, this configuration may be the cause of the W4f intermixing peak, which is fitted with a Doniach–Sunjic lineshape in Fig. 4. A look at the 2/3 ML model suggests that interchanging the second layer W and Ru atoms may also lead to a significant SCLS. However, a surface W atom interacts with only 6 Ru atoms, which suggests that Ru forms islands at submonolayer coverages.

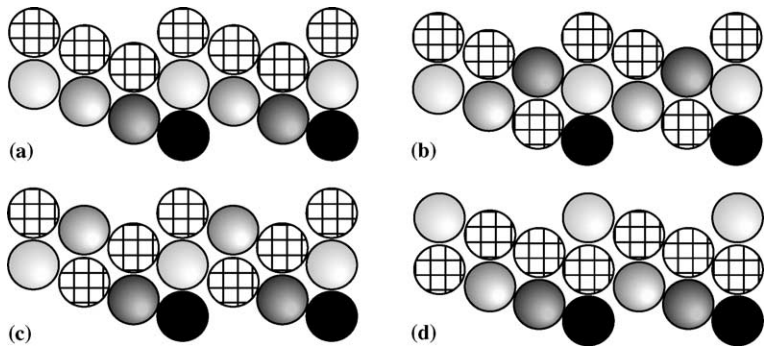

Fig. 19. Illustration of the intermixing of 1 ML Ru on W(1 1 1). (a) 1 ML Ru/W(1 1 1), (b) third layer interchange of W and Ru atoms, (c) second layer interchange of W and Ru atoms and (d) first layer interchange of W and Ru atoms.

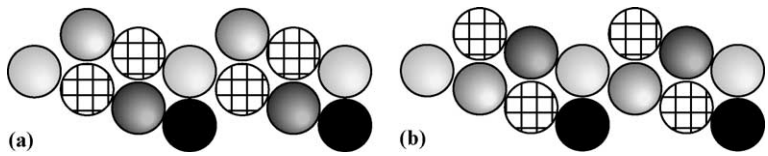

Fig. 20. Intermixing of 2/3 ML Ru on W(1 1 1). (a) interchange of second layer W and Ru atoms and (b) interchange third layer W and Ru atoms.

Within these islands, 1 ML coverage may be attained and therefore the 1 ML-interchange model is appropriate; this would explain the appearance of the observed feature at less than 1 ML doses. Growth of Pt/W(1 1 1) islands with local coverage of 1 ML is seen for Pt coverages between 0.7 and 1.0 ML by Pelhos et al. [16].

A model similar to the above has been created for the (2 1 1) surface. The coordination for the clean (2 1 1) surface is shown below:

$$\text{Layer 1} = 5W_{NN} + 3W_{NNN} + 3Vac_{NN} + 3Vac_{NNN}$$

$$\text{Layer 2} = 7W_{NN} + 5W_{NNN} + 1Vac_{NN} + 1Vac_{NNN}$$

The major difference between the two layers is the two extra W nearest neighbor atoms for layer 2 and two extra nearest neighbor "vacuum atoms" in layer 1. This combination provides the difference in binding energy observed between the two layers for the clean W(2 1 1) surface of the $W4f_{7/2}$ SXPX spectrum in Fig. 13.

A complete physical monolayer produces (at most) $3Ru_{NN}$ and $3Ru_{NNN}$ and this would again account for the intermixing peak with a binding energy shift of 280 meV from the bulk feature of (Fig. 12). Applying the same interchange method as used for the (1 1 1) surface the coordination produces an interaction that has an equivalent number of Ru_{NN} and Ru_{NNN} with the 1 ML coverage observed above. If every second atom in the second layer is interchanged with the Ru atom above it the coordination changes to give $5Ru_{NN}$ and $3W_{NN}$. Additionally, this interchange has an interesting structure that may be a possible stable alloy state. Although the analysis of the (2 1 1) surface is not as striking as the (1 1 1) surface, but it enables a basis for further understanding of the surface intermixing process.

6. Conclusion

Ruthenium has been shown to induce faceting of W(1 1 1) upon annealing. Dosing Ru at room temperature onto both W(1 1 1) and W(2 1 1) causes intermixing of the Ru and W atoms to occur in the surface layer, even for fractional monolayer coverages. Upon annealing above ~570 K, for Ru coverages > 1 ML, alloy features begin to develop, indicating the initial formation of a stable W–Ru phase in the overlayer. Tungsten atoms interchange with or diffuse into the Ru overlayer. At 770 K, faceting of the W(1 1 1) surface is initiated and optimal faceting of the surface occurs at ~970 K. Between 970 and 1330 K, the surface restructures and clustering of the alloys occurs; in this process, the Ru–W interface is uncovered which causes the intermixing peak observed for coverages less than a monolayer to reappear. At temperatures higher than 1300 K the clustered alloys destabilize, prior to the onset of desorption of Ru. The phenomenon of intermixing for fractional monolayer coverages is distinctly different from other overlayers (Pt, Pd, Rh) W(1 1 1) and W(1 1 2), whereas alloying of multilayer Ru is similar to that observed for Pt, Pd, Ru on W(1 1 1) and W(1 1 2).

Acknowledgements

This work has been supported in part by the US Army Research Office and the US Department of Energy. M.J. Gladys acknowledges support from the Australian–American Fulbright Association. The National Synchrotron Light Source at Brookhaven National Laboratory is supported by the US Department of Energy, Division of Materials Sciences and Division of Chemical Sciences (DOE contract no. DOE-AC02-76CH00016).

References

[1] N.J. Taylor, Surf. Sci. 2 (1964) 544.
[2] J.C. Tracy, J.M. Blakely, Surf. Sci. 13 (1968) 313.
[3] F. Bonczek, T. Engel, E. Bauer, Surf. Sci. 97 (1980) 595.
[4] T.E. Madey, J. Guan, C.-H. Nien, C.-Z. Dong, H.-S. Tao, R.A. Campbell, Surf. Rev. Lett. 3 (1996) 1315.
[5] T.E. Madey, C.-H. Nien, K. Pelhos, J.J. Kolodziej, I.M. Abdelrehim, H.-S. Tao, Surf. Sci. 438 (1999) 191.
[6] J. Guan, R.A. Campbell, T.E. Madey, Surf. Sci. 341 (1995) 157–173.
[7] K.-J. Song, J.-C. Lin, M.-Y. Lai, Y.-L. Wang, Surf. Sci. 327 (1995) 17.
[8] K. Pelhos, T.E. Madey, R. Blaszczyszyn, Surf. Sci. 426 (1999) 61.
[9] A. Cetronio, J.P. Jones, Surf. Sci. 2 (1964) 496.

[10] K.-J. Song, W.-R. Chen, V. Yeh, Y.-W. Liao, P.T. Tsao, M.-T. Lin, Surf. Sci. 478 (2001) 145.
[11] G. Che, C.T. Chan, C.H. Kuo, T.C. Leung, Phys. Rev. Lett. 79 (1997) 4230.
[12] H.-S. Tao, T.E. Madey, J.E. Rowe, Surf. Sci. 407 (1998) L640–L646.
[13] J.J. Kolodziej, K. Pelhos, I.M. Abdelrehim, J.W. Keister, J.E. Rowe, T.E. Madey, Prog. Surf. Sci. 59 (1999) 117.
[14] J.J. Kolodziej, J.W. Keister, J.E. Rowe, T.E. Madey, Phys. Rev. B 62 (2000) 5150.
[15] J.J. Kolodziej, J.W. Keister, J.E. Rowe, T.E. Madey, Phys. Rev. B 65 (2002) 075413-1.
[16] K. Pelhos, T.E. Madey, J.B. Hannon, G.L. Kellogg, Surf. Rev. Lett. 6 (1999) 767.
[17] S. Doniach, M. Sunjic, J. Phys. C 3 (1970) 285.
[18] G.K. Wertheim, P.H. Citrin, J.F. van der Veen, Phys. Rev. B 30 (1984) 4343.
[19] K.-J. Song, C.-Z. Dong, T.E. Madey, Langmuir 7 (1991) 3019.
[20] K.-J. Song, R.E. Demmin, C.-Z. Dong, E. Garfunkel, T.E. Madey, Surf. Sci. 227 (1990) L79.
[21] A.V. Ruban, H.L. Skriver, J.K. Norskov, Phys. Rev. B 59 (1999) 1–11.
[22] R.E. Watson, M.L. Perlman, Phys. Scr. 21 (1980) 527.
[23] R.E. Watson, L.H. Bennett, Phys. Rev. Lett. 143 (1979) 1130.
[24] A. Christensen, A.V. Ruban, et al., Phys. Rev. B 56 (1997) 5822.
[25] C.-H. Nien, T.E. Madey, Surf. Sci. 380 (1997) L527.